

Integrated lithium niobate electro-optic modulators operating at CMOS-compatible voltages

Cheng Wang^{1,2,6}, Mian Zhang^{1,6}, Xi Chen³, Maxime Bertrand^{1,4}, Amirhassan Shams-Ansari^{1,5}, Sethumadhavan Chandrasekhar³, Peter Winzer³ & Marko Lončar^{1*}

Electro-optic modulators translate high-speed electronic signals into the optical domain and are critical components in modern telecommunication networks^{1,2} and microwave-photonic systems^{3,4}. They are also expected to be building blocks for emerging applications such as quantum photonics^{5,6} and non-reciprocal optics^{7,8}. All of these applications require chip-scale electro-optic modulators that operate at voltages compatible with complementary metal–oxide–semiconductor (CMOS) technology, have ultra-high electro-optic bandwidths and feature very low optical losses. Integrated modulator platforms based on materials such as silicon, indium phosphide or polymers have not yet been able to meet these requirements simultaneously because of the intrinsic limitations of the materials used. On the other hand, lithium niobate electro-optic modulators, the workhorse of the optoelectronic industry for decades⁹, have been challenging to integrate on-chip because of difficulties in microstructuring lithium niobate. The current generation of lithium niobate modulators are bulky, expensive, limited in bandwidth and require high drive voltages, and thus are unable to reach the full potential of the material. Here we overcome these limitations and demonstrate monolithically integrated lithium niobate electro-optic modulators that feature a CMOS-compatible drive voltage, support data rates up to 210 gigabits per second and show an on-chip optical loss of less than 0.5 decibels. We achieve this by engineering the microwave and photonic circuits to achieve high electro-optical efficiencies, ultra-low optical losses and group-velocity matching simultaneously. Our scalable modulator devices could provide cost-effective, low-power and ultra-high-speed solutions for next-generation optical communication networks and microwave photonic systems. Furthermore, our approach could lead to large-scale ultra-low-loss photonic circuits that are reconfigurable on a picosecond timescale, enabling a wide range of quantum and classical applications^{5,10,11} including feed-forward photonic quantum computation.

Future photonic systems require modulators with a CMOS-compatible drive voltage, a large bandwidth, a low optical insertion loss, a high extinction ratio, excellent signal quality and compatibility with large-scale manufacturing. Because discrete lithium niobate (LN) modulators are difficult to integrate, many other photonic platforms compatible with microfabrication processes have been pursued instead, including those based on silicon^{1,12,13}, indium phosphide^{14,15}, polymers^{16,17} and plasmonics¹⁸. These have shown excellent scalability and distinct performance merits, including the potential for integration with CMOS electronics (Si), low drive voltages (InP, polymer), ultra-high bandwidths (polymer, plasmonics) and small footprints (Si, plasmonics). Although the integration problem has been greatly alleviated in these platforms, a modulator that simultaneously meets all desired performance aspects remains elusive because of the non-ideal electro-optic properties of the underlying materials.

The material properties of LN are well suited for realizing ultra-fast modulation, low-voltage operation and low optical losses at the same

time. The strong electro-optic (Pockels) effect in LN leads to a linear change of its refractive index in response to an applied voltage, on femtosecond timescales¹⁹. Although it has been known for some time that microstructured LN devices can provide better modulator performance²⁰, most commercial LN modulators are still based on titanium-indiffusion or proton-exchange waveguides, because LN is notoriously difficult to etch⁹. These waveguides typically have a low refractive index contrast Δn of around 0.02 between core and cladding, resulting in a large optical mode size²¹. The weak optical confinement requires metal electrodes to be spaced far apart from the optical waveguide (about 10 μm), lowering the electro-optic efficiency. As a result, LN modulators today are much larger in size and require much higher drive voltages than the material is capable of supporting.

In recent years, the LN-on-insulator platform has emerged as a promising candidate for integrated high-performance modulators. In this approach, a single-crystal, submicrometre-thick LN film is bonded on top of a low-index substrate (silicon dioxide, SiO_2), and waveguides are created by dry etching the LN device layer²². This has led to a range of LN photonic devices with high index contrast of >0.7 and tightly confined optical modes^{23–29}. Electro-optic modulators with promising electro-optic efficiencies have been demonstrated^{25–27,29}. However, the actual switching voltages, bandwidths and optical losses in these demonstrations still suffer from critical trade-offs, limited by non-ideal etching, reduced overlap between electrical and optical fields, and/or the inefficient microwave signal delivery. Whether it is possible to simultaneously achieve a low on/off switching voltage, an ultra-high bandwidth and a low optical loss in LN modulators has remained an outstanding question.

Here we demonstrate monolithically integrated LN electro-optic modulators (Fig. 1) that overcome such trade-offs, featuring a switching voltage of 1.4 V while supporting very high bandwidths. Our integrated modulators operate in a travelling-wave Mach-Zehnder interferometer (MZI) configuration that uses highly confined co-propagating microwave and optical fields with matched group velocities and low propagation losses. A 50:50 Y-junction splits the input light into two LN optical waveguides that form the arms of the MZI. The optical waveguides run through the dielectric gaps of a ground-signal-ground coplanar microwave strip line (Fig. 1d). As a result, the microwave electric field has opposite signs across the two LN waveguides, thus inducing (through the Pockels effect) an optical phase delay on one arm and an optical phase advance on the other. This optical phase difference results in constructive/destructive interference at the output 50:50 Y-junction, and thereby an amplitude modulation of the output optical signal (Fig. 1c). An important figure of merit for MZI modulators is the half-wave voltage (V_π), defined as the voltage required to induce a π -phase difference between the two modulator arms, changing the optical transmission from maximum to minimum. For a device with 20-mm-long microwave strip line electrodes, we measure a low V_π of 1.4 V (Fig. 1c), which allows the modulator to be directly driven by a CMOS circuit. Importantly, our devices also

¹John A. Paulson School of Engineering and Applied Sciences, Harvard University, Cambridge, MA, USA. ²Department of Electronic Engineering, City University of Hong Kong, Kowloon, Hong Kong, China. ³Nokia Bell Labs, Holmdel, NJ, USA. ⁴LP2N, Institut d'Optique Graduate School, CNRS, University of Bordeaux, Talence, France. ⁵Department of Electrical Engineering and Computer Science, Howard University, Washington, DC, USA. ⁶These authors contributed equally: Cheng Wang, Mian Zhang. *e-mail: loncar@seas.harvard.edu

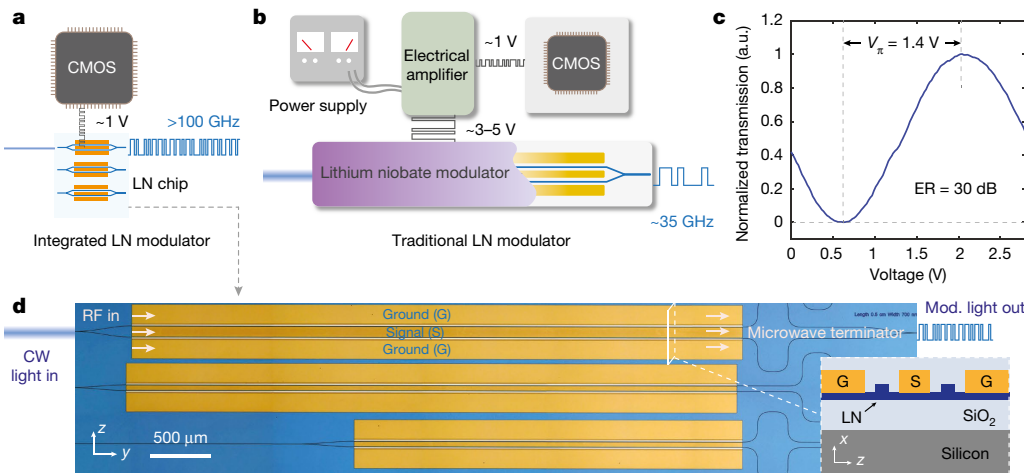


Fig. 1 | Nanophotonic LN modulators compatible with CMOS drive voltages. **a, b**, Schematic comparison of the data-transmitting set-ups for integrated (**a**) and traditional (**b**) LN modulators. The nanophotonic LN modulator (**a**) supports direct CMOS driving with high bandwidths (>100 GHz), while traditional modulators (**b**) require large and power-consuming electrical driver amplifiers and have limited bandwidths (approximately 35 GHz). **c**, Normalized optical transmission of a 20-mm

feature a high optical power extinction ratio of about 30 dB between on and off states (see Methods).

In the travelling-wave electrode configuration, longer microwave strip lines could be used to induce a larger optical phase shift, thus reducing the V_π value. However, this degrades the electro-optic bandwidth, owing to exacerbated mismatch between microwave and optical velocities, and larger microwave loss. This contradictory requirement on electrode length results in a voltage–bandwidth trade-off⁹. In traditional LN modulators, the large optical mode size requires the metal electrodes to be placed far from the optical waveguides, and very long electrodes are required to reduce the voltage to even modest levels. As a result, the voltage–bandwidth performance of these modulators is typically limited to V_π about 3.5 V and bandwidth about 35 GHz, requiring power-consuming electrical amplifiers to drive them (Fig. 1b)⁹.

In contrast, the thin-film LN modulator can overcome the bandwidth–voltage performance limitation by maximizing the electro-optic overlap using photonic structures with a strong optical confinement^{25,26,29}. Owing to the increased modulation efficiency, our devices are much shorter (ranging from 5 mm to 20 mm) than conventional counterparts (typically >5 cm), while allowing for V_π values at CMOS levels (Fig. 1a). Moreover, as the optical mode is highly localized in the submicrometre waveguide region whereas the microwave mode resides largely in the substrate, it is possible to engineer the microwave and

device as a function of the applied voltage, showing a low half-wave voltage of 1.4 V. The measured extinction ratio is 30 dB. **d**, Microscope image of the fabricated chip consisting of three Mach–Zehnder modulators with various microwave signal line widths and device lengths. The thin-film configuration allows for maximum field overlap and velocity matching between microwave and optics. Inset shows the cross-sectional schematic of the nanophotonic LN modulator. Mod., modulated; RF, radiofrequency.

optical group velocities independently, by designing the layer thicknesses of the LN/SiO₂/Si stack (see Methods). As a result, our devices can maintain velocity matching between the optical and the microwave signals at very high microwave frequencies without sacrificing the electro-optic overlap. Figure 2a presents the measured small-signal electro-optic response of the 20-mm-long device, showing a high 3-dB bandwidth of >45 GHz. These devices also possess ultra-low on-chip optical losses of <0.5 dB (see Methods)²⁸.

We use the low-voltage, high-bandwidth and low-loss integrated modulators to demonstrate data modulation at 70 Gbit s⁻¹ directly driven by a CMOS circuit (Fig. 2b–d). High-speed electrical signals are generated by a CMOS digital-to-analogue conversion (DAC) circuit and directly used to drive our modulator without an electrical amplifier. Figure 2c, d shows measured constellation diagrams (Fig. 2c, d, left) from a coherent receiver, which recovers both amplitude and phase of the output optical field at each data-sampling instant. The vertical and horizontal axes correspond to the in-phase and quadrature components of the measured optical fields. Distinct constellations with fewer overlapping data points between ‘0’ and ‘1’ correspond to the desired lower bit-error ratios (BER). The eye diagrams (Fig. 2c, d right) are generated by up-sampling the received digital data for better visualization (see Methods). Low BERs correspond to clear separation between the discrete data levels at the sampling time (i.e. middle of the eye diagrams). At a peak-to-peak drive voltage (V_{pp}) of 200 mV, the modulated optical

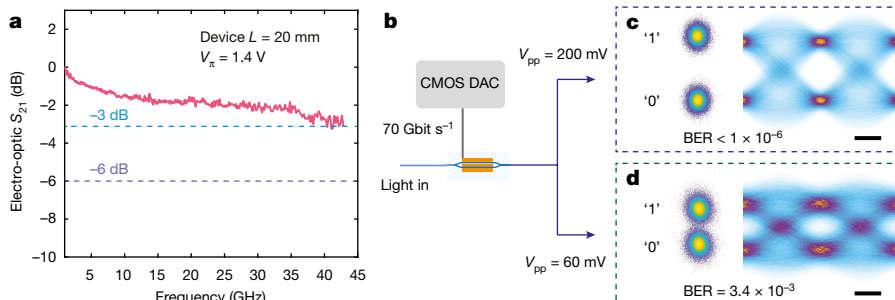


Fig. 2 | Directly CMOS-driven data transmission at 70 Gbit s⁻¹. **a**, Small-signal electro-optic response of a device with an active modulation length of 20 mm, showing a high 3-dB bandwidth of >45 GHz. S_{21} , transmission coefficient of the scattering matrix. **b**, The device is used for data-transmission experiments at a rate of 70 Gbit s⁻¹ rate, directly

driven by a CMOS circuit. **c, d**, Measured constellation diagrams obtained with a coherent receiver (left), and the reconstructed eye diagrams (right). At peak-to-peak voltages of 200 mV (**c**) and 60 mV (**d**), the measured BERs are $<1 \times 10^{-6}$ and 3.4×10^{-3} , respectively. The eye diagrams are obtained by up-sampling the received data for better visualization. Scale bars, 5 ps.

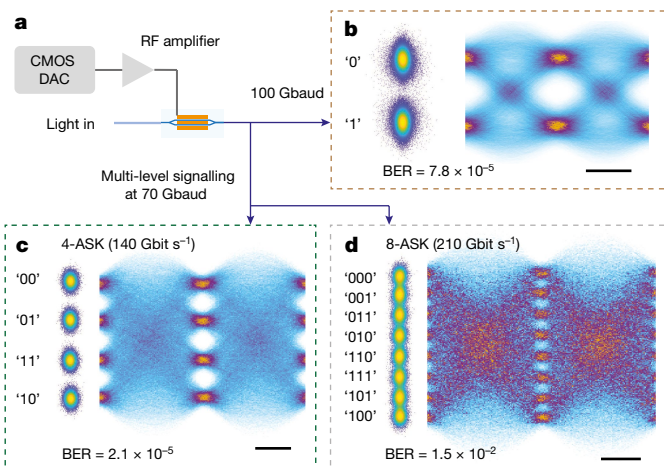


Fig. 3 | Ultra-high-speed data transmission at 100 Gbaud and 210 Gbit s⁻¹. **a**, Binary signals at an ultra-high symbol rate of 100 Gbaud, as well as multi-level signals at 70 Gbaud, are generated from a CMOS circuit and amplified to a peak-to-peak voltage of 2.5 V to drive the integrated modulator. **b**, Constellation diagram and reconstructed eye diagram of data transmission at 100 Gbaud. The relatively high BER of 7.8×10^{-5} is limited by the electrical signal quality at this ultra-high speed. **c**, **d**, Multi-level data modulation at a symbol rate of 70 Gbaud. The four-level (**c**) and eight-level (**d**) ASK signals enable even higher data-transmission rates of 140 Gbit s^{-1} and 210 Gbit s^{-1} , respectively. The measured BERs are 2.1×10^{-5} and 1.5×10^{-2} , respectively. Scale bars, 5 ps.

signal yields error-free performance within the 1.1×10^6 captured signal bits; that is, $\text{BER} < 1 \times 10^{-6}$ (Fig. 2c). In this case, the electrical energy dissipation within our modulator is 0.37 fJ bit^{-1} (see Methods). The system can also operate at a further reduced driving voltage of $V_{\text{pp}} = 60 \text{ mV}$, with a BER of 3.4×10^{-3} (Fig. 2d). In this case, the electrical energy dissipation of the modulator is further reduced to 37 aJ bit^{-1} . We note that the overall energy consumption of the complete data-transmission system is dominated by off-chip components, including CMOS DAC, laser, receiver set-up and analogue-to-digital converters. It is important to consider the whole system when assessing the overall system energy requirements.

The high electro-optic bandwidth and excellent signal fidelity of our modulator allow for data transmission at even higher rates, currently up to 210 Gbit s^{-1} . To achieve this, we amplify the electrical signals from the CMOS DAC to a V_{pp} of about 2.5 V (Fig. 3a). We first test our modulator at an ultra-high symbol rate of 10^11 symbols per second (100 Gbaud) (Fig. 3b; see Methods)³⁰. The BER of 7.8×10^{-5} in this case is limited by distortion from the electrical source at high frequencies: the electrical BER at 100 Gbaud without any electrical-to-optical-to-electrical conversion is 3.6×10^{-5} (see Methods). We then use multi-level modulation formats at 70 Gbaud to further increase the data rates and to interrogate the signal quality (that is, signal-to-noise ratio, SNR) of our modulator. Using four-level amplitude shift keying (4-ASK)—that is, encoding two bits in each symbol—we can achieve a data-transmission rate of 140 Gbit s^{-1} , with a low BER of 2.1×10^{-5} . In the case of 8-ASK (three bits per symbol), the modulator transmits a total data rate of 210 Gbit s^{-1} . The measured BER of 1.5×10^{-2} is within the tolerance of forward error correction with a 20% overhead (tolerable BER = 1.9×10^{-2}). For the 8-ASK modulation, the electrical energy dissipation of our modulator is 14 fJ bit^{-1} (see Methods). The high SNR demonstrated here results from a combination of high extinction ratio, low optical loss, linear electro-optic response and the absence of modulation-induced absorption. This further indicates that our devices have maintained the excellent signal fidelity of conventional LN modulators.

We show that the integrated LN platform offers greatly improved overall performance (voltage, bandwidth and optical loss) over traditional LN modulators and other material platforms. By reducing the device

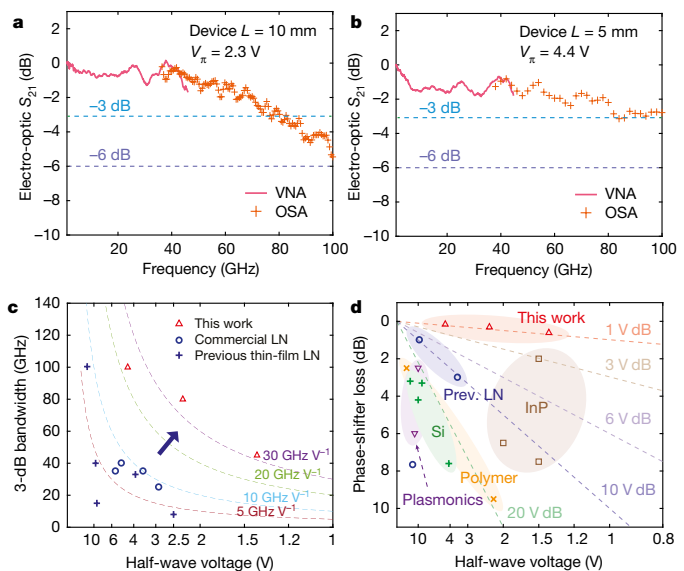


Fig. 4 | Towards ultimate modulator performance. **a**, **b**, Electro-optic responses of a 10-mm (**a**) and a 5-mm (**b**) device, showing ultra-high 3-dB bandwidths of 80 GHz and 100 GHz, respectively. The low-frequency (red line) and high-frequency (orange crosses) measurements are performed using a vector network analyser (VNA) and an optical spectrum analyser (OSA), respectively. **c**, Comparison of key modulator figure of merit (BW/V_π, ratio between 3-dB electro-optic bandwidth BW and half-wave voltage V_π) for this work, for state-of-the-art commercial LN modulators and for previous thin-film LN modulators, showing much higher BW/V_π values of about 30 GHz V^{-1} for this work. The dotted lines correspond to constant values of BW/V_π. **d**, In comparison with other material platforms with high bandwidths, the integrated LN modulators show much lower V_π and much lower on-chip optical loss at the same time. The optical losses in the active modulation regions are used for fair comparison between different platforms. Detailed references for the data shown in **c** and **d** can be found in the Methods.

length to 10 mm and 5 mm, we further expand the 3-dB electro-optic bandwidths to 80 GHz and 100 GHz, respectively (Fig. 4a, b), which are measured using an optical spectrum analyser (see Methods)³¹. The measured V_π values for these devices are 2.3 V and 4.4 V, respectively (see Methods). Further optimizing the microwave losses of the transmission lines could allow for electro-optic bandwidths of $>100 \text{ GHz}$ while maintaining a CMOS-level voltage. Nevertheless, our modulators already represent better voltage-bandwidth performance (about 30 GHz V^{-1}) than commercial LN modulators and previously reported thin-film LN devices, as illustrated in Fig. 4c. The ultra-high bandwidth of these modulators could allow for data operation beyond 200 Gbaud. Furthermore, in contrast to other high-speed modulator platforms in which the optical materials or modulation mechanisms are often inherently lossy, our integrated LN platform breaks the traditional trade-off between modulation voltage and propagation loss, allowing for low optical loss and low V_π at the same time (Fig. 4d). Given the voltage-loss performance of our platform, it should be possible to use even longer devices to further reduce the V_π to well below 1 V while maintaining an on-chip insertion loss of below 1 dB.

The results presented here show that ultra-high-performance integrated LN modulators have the properties desired for future high-bandwidth and low-power-consumption data communications. By combining the excellent signal fidelity with advanced in-phase/quadrature (I/Q) modulator designs, a single integrated LN modulator could transmit more than 1 Tb s^{-1} of data per polarization, using, for example, 64-quadrature amplitude modulation (64-QAM) at 200 Gbaud. Using meandering optical waveguides and microwave transmission lines could lead to modulators with even smaller footprint while maintaining CMOS-compatible voltages. This could open opportunities for direct optoelectronic integration of switching components with

application-specific integrated circuits². Furthermore, the low optical and microwave losses, linear electro-optic response, scalability and the ability to be integrated with other photonic components (such as filters and delay lines) could inspire a new generation of active integrated optoelectronic circuits that can be reconfigured on a picosecond timescale using attojoules of electrical energy. These applications include large-scale gigahertz switching networks for quantum photonics⁵, radio signal processing in the optical domain for microwave photonics⁴, self-aware optical networks¹⁰, non-reciprocal devices⁸, topological photonic circuits³² and photonic neural networks¹¹.

Online content

Any methods, additional references, Nature Research reporting summaries, source data, statements of data availability and associated accession codes are available at <https://doi.org/10.1038/s41586-018-0551-y>.

Received: 27 April 2018; Accepted: 25 July 2018;

Published online 24 September 2018.

1. Reed, G. T., Mashanovich, G., Gardes, F. Y. & Thomson, D. J. Silicon optical modulators. *Nat. Photon.* **4**, 518–526 (2010).
2. Miller, D. A. B. Attojoule optoelectronics for low-energy information processing and communications. *J. Lightwave Technol.* **35**, 346–396 (2017).
3. Fortier, T. M. et al. Generation of ultrastable microwaves via optical frequency division. *Nat. Photon.* **5**, 425–429 (2011).
4. Ghelfi, P. et al. A fully photonic-based coherent radar system. *Nature* **507**, 341–345 (2014).
5. O'Brien, J. L. Optical quantum computing. *Science* **318**, 1567–1570 (2007).
6. Kues, M. et al. On-chip generation of high-dimensional entangled quantum states and their coherent control. *Nature* **546**, 622–626 (2017).
7. Yu, Z. & Fan, S. Complete optical isolation created by indirect interband photonic transitions. *Nat. Photon.* **3**, 91–94 (2009).
8. Tzang, L. D., Fang, K., Nussenzveig, P., Fan, S. & Lipson, M. Non-reciprocal phase shift induced by an effective magnetic flux for light. *Nat. Photon.* **8**, 701–705 (2014).
9. Wooten, E. L. et al. A review of lithium niobate modulators for fiber-optic communications systems. *IEEE J. Sel. Top. Quantum Electron.* **6**, 69–82 (2000).
10. Miller, D. A. B. Sorting out light. *Science* **347**, 1423–1424 (2015).
11. Shen, Y. et al. Deep learning with coherent nanophotonic circuits. *Nat. Photon.* **11**, 441–446 (2017).
12. Xu, Q., Schmidt, B., Pradhan, S. & Lipson, M. Micrometre-scale silicon electro-optic modulator. *Nature* **435**, 325–327 (2005).
13. Sun, C. et al. Single-chip microprocessor that communicates directly using light. *Nature* **528**, 534–538 (2015).
14. Ogiso, Y. et al. Over 67 GHz bandwidth and 1.5 V InP-based optical IQ modulator with n-i-p-n heterostructure. *J. Lightwave Technol.* **35**, 1450–1455 (2017).
15. Aoki, M. et al. InGaAs/InGaAsP MQW electroabsorption modulator integrated with a DFB laser fabricated by band-gap energy control selective area MOCVD. *IEEE J. Quantum Electron.* **29**, 2088–2096 (1993).
16. Koeber, S. et al. Femtojoule electro-optic modulation using a silicon–organic hybrid device. *Light Sci. Appl.* **4**, e255 (2015).
17. Lee, M. et al. Broadband modulation of light by using an electro-optic polymer. *Science* **298**, 1401–1403 (2002).
18. Haffner, C. et al. Low-loss plasmon-assisted electro-optic modulator. *Nature* **556**, 483–486 (2018).
19. Boyd, R. W. *Nonlinear Optics* (Academic, Cambridge, 2003).
20. Janner, D., Tulli, D., García-Granda, M., Belmonte, M. & Pruneri, V. Micro-structured integrated electro-optic LiNbO₃ modulators. *Laser Photonics Rev.* **3**, 301–313 (2009).
21. Schmidt, R. V. & Kaminow, I. P. Metal-diffused optical waveguides in LiNbO₃. *Appl. Phys. Lett.* **25**, 458–460 (1974).
22. Poberaj, G., Hu, H., Sohler, W. & Günter, P. Lithium niobate on insulator (LNOI) for micro-photonic devices. *Laser Photonics Rev.* **6**, 488–503 (2012).
23. Liang, H., Luo, R., He, Y., Jiang, H. & Lin, Q. High-quality lithium niobate photonic crystal nanocavities. *Optica* **4**, 1251–1258 (2017).
24. Wang, J. et al. High-Q lithium niobate microdisk resonators on a chip for efficient electro-optic modulation. *Opt. Express* **23**, 23072–23078 (2015).
25. Wang, C., Zhang, M., Stern, B., Lipson, M. & Lončar, M. Nanophotonic lithium niobate electro-optic modulators. *Opt. Express* **26**, 1547–1555 (2018).
26. Rao, A. et al. High-performance and linear thin-film lithium niobate Mach-Zehnder modulators on silicon up to 50 GHz. *Opt. Lett.* **41**, 5700–5703 (2016).
27. Chen, L., Xu, Q., Wood, M. G. & Reano, R. M. Hybrid silicon and lithium niobate electro-optical ring modulator. *Optica* **1**, 112–118 (2014).
28. Zhang, M., Wang, C., Cheng, R., Shams-Ansari, A. & Lončar, M. Monolithic ultra-high-Q lithium niobate microring resonator. *Optica* **4**, 1536–1537 (2017).
29. Weigel, P. O. et al. Hybrid silicon photonic-lithium niobate electro-optic Mach-Zehnder modulator beyond 100 GHz. Preprint at <https://arxiv.org/abs/1803.10365> (2018).
30. Chen, X. et al. All-electronic 100-GHz bandwidth digital-to-analog converter generating PAM signals up to 190 Gbaud. *J. Lightwave Technol.* **35**, 411–417 (2017).
31. Chen, X. et al. Characterization of electro-optic bandwidth of ultra-high speed modulators. In *2017 Optical Fiber Communications Conference and Exhibition* 1–3 (2017); <https://doi.org/10.1364/OFC.2017.Tu2H.7>
32. Yuan, L., Xiao, M., Lin, Q. & Fan, S. Synthetic space with arbitrary dimensions in a few rings undergoing dynamic modulation. *Phys. Rev. B* **97**, 104105 (2018).

Acknowledgements We thank J. Khan for discussions on the LN platform, H. Majedi for help with the equipment, and C. Reimer, S. Bogdanović, L. Shao and B. Desiatov for feedback on the manuscript. This work is supported in part by the National Science Foundation (NSF) (ECCS1609549, ECCS-1740296 E2CDA and DMR-1231319) and by Harvard University Office of Technology Development (Physical Sciences and Engineering Accelerator Award). Device fabrication is performed at the Harvard University Center for Nanoscale Systems, a member of the National Nanotechnology Coordinated Infrastructure Network, which is supported by the NSF under ECCS award no. 1541959.

Reviewer information *Nature* thanks M. Hochberg and the other anonymous reviewer(s) for their contribution to the peer review of this work.

Author contributions C.W., M.Z., X.C., P.W. and M.L. conceived the experiment. C.W., M.Z. and A.S. fabricated the devices. M.Z. and M.B. performed numerical simulations. C.W., M.Z., X.C. and S.C. carried out the device characterization. C.W. wrote the manuscript with contribution from all authors. P.W. and M.L. supervised the project.

Competing interests C.W., M.Z. and M.L. are involved in developing lithium niobate technologies at HyperLight Corporation.

Additional information

Extended data is available for this paper at <https://doi.org/10.1038/s41586-018-0551-y>.

Reprints and permissions information is available at <http://www.nature.com/reprints>.

Correspondence and requests for materials should be addressed to M.L.

Publisher's note: Springer Nature remains neutral with regard to jurisdictional claims in published maps and institutional affiliations.

METHODS

Device fabrication. Devices are fabricated from a commercial x-cut LN-on-insulator wafer (NANOLN), in which a 600-nm device layer sits on top of a SiO₂/Si-stack substrate. We use electron-beam lithography (EBL) and Ar⁺-based reactive ion etching to define optical waveguides and MZIs in thin-film LN, using a similar process as described in our previous work²⁸. A 1.5-μm-thick polymethyl methacrylate (PMMA) EBL resist is spin-coated and exposed, again using EBL with alignment, to define the microwave transmission line patterns. The PMMA resist is used for a lift-off process to produce the 1.1-μm-thick gold strip lines. High-precision alignment between the two layers is required to prevent excessive propagation loss from the metal electrodes. The structures are then cladded with an 800-nm-thick SiO₂ layer by plasma-enhanced chemical vapour deposition. Finally, the chip edges are diced and polished to improve the fibre-to-chip coupling.

Electro-optic characterization. Electro-optic characterization is performed in the telecommunications C-band using a tunable-wavelength laser source (Santec TSL-510). A three-paddle polarization controller is used to ensure transverse-electric mode excitation. Light is butt-coupled into and out of the chip under test using tapered lensed fibres, with a coupling loss of about 5 dB per facet. We have previously done extensive studies on the dependence of waveguide propagation loss on the waveguide geometry²⁸. In the current work, we use a waveguide top width of 800 nm to ensure single-mode operation. The corresponding propagation loss is approximately 0.2 dB cm⁻¹, higher than the best value reported in our previous work²⁸ owing to more sidewall scattering losses in the narrower waveguide. This results in an overall on-chip phase-shifter insertion loss of <0.5 dB, as estimated by comparing fibre-to-fibre transmission signals for our modulators (total waveguide lengths >3 cm) and bare waveguides with short total lengths. Within the measurement uncertainty (± 0.5 dB), we did not observe measurable loss difference for the two types of devices, thus extracting an upper bound of on-chip losses of 0.5 dB. For our V_π measurement, a triangular voltage signal ($V_{pp} = 5$ V) is used to drive the modulator while the optical transmission signal is monitored in real time. A pair of high-speed microwave probes (GGB) is used to deliver the modulation signal to the input port of the transmission line, and to terminate the output of the transmission line with a 50-Ω load. The electro-optic response below 45 GHz is measured with a vector network analyser in a set-up similar to that used in our previous work²⁵.

Extended Data Fig. 1 shows the half-wave voltage measurements for three devices characterized, with active device lengths of 20 mm, 10 mm and 5 mm. The inset of Extended Data Fig. 1a shows the optical transmission on a logarithmic scale, indicating a measured device extinction ratio of 30 dB. The high experimental extinction ratio also implies a high fabrication quality for the Y-junctions, with a nearly ideal 50:50 split ratio. The extinction ratio could be further improved by using directional couplers. The measured V_π values for the 10-mm and 5-mm devices are 2.3 V and 4.4 V, corresponding to voltage-length products of 2.3 V cm and 2.2 V cm, respectively.

Ultra-high-speed device characterization. The electro-optic response from 35 GHz to 100 GHz is tested with an optical spectrum analyser (Extended Data Fig. 2a)³¹. A sinusoidal signal (f_i) from a high-speed synthesizer (up to 50 GHz) is used to drive a commercial LN Mach-Zehnder modulator, which has a 3-dB bandwidth of about 35 GHz, with the frequency response gradually rolling off thereafter. The modulator is biased at the transmission null to suppress the carrier frequency, resulting in an output optical signal with two sidebands separated by twice the input frequency ($2f_i$). A 100-GHz photodetector is used to beat the two sidebands and generate a microwave signal up to 100 GHz, which is subsequently used to drive the modulator under test. The modulator optical response is measured by monitoring the sideband power in the optical spectrum analyser. We calibrate the synthesizer output power, the electro-optic response of the commercial Mach-Zehnder modulator and the 100-GHz photodetector response over the frequency range of interest to ensure an accurate characterization of our devices. Note that the actual measurement is performed using a pair of 67-GHz probes (one for microwave signal modulation and the other for 50-Ω termination). The frequency response of the probes is not de-embedded due to the lack of manufacturer data. Therefore, the bandwidth reported here is a lower bound for our devices.

The measurement set-up for high-speed data modulation is shown in Extended Data Fig. 2b. Electrical signals up to 70 Gbaud are directly generated from a CMOS DAC circuit (Socionext OOLA DAC, 3-dB analogue bandwidth 15 GHz, 13-dB analogue bandwidth 35 GHz). The transmitter uses a digital pulse-shaping filter to limit the signal to its Nyquist bandwidth (for example, 35 GHz electrical bandwidth for a 70-Gbaud signal). The electrical signals from the DAC have a peak-to-peak voltage of ~ 0.2 V and can be further amplified or attenuated before being used to drive the modulator under test. The modulator is biased at the transmission null point to generate binary phase-shift keying, 4-ASK and 8-ASK³³. The output optical signal is mixed with a local oscillator in an optical hybrid and is sent into a single-polarization phase-diversity coherent receiver with a pair of balanced 45-GHz photodetectors to extract the in-phase and quadrature components of the modulated light field. Digitized data are collected using an 80-GSa/s real-time oscilloscope

with an analogue bandwidth of 63 GHz (Keysight DSOZ634A). The collected data are post-processed using least-mean-square adaptive filters to equalize the optical channel response, and to generate the constellation diagrams. The eye diagrams are plotted by up-sampling the real part of the recovered constellations using an interpolation filter for better visualization. At 100 Gbaud, the electrical signal is generated by up-conversion and interleaving two 35-GHz electrical signals³⁰. Extended Data Fig. 3 shows the electrical eye diagram at 100 Gbaud, with a BER of 3.6×10^{-5} , limited by the signal distortion from the electronic circuit. This electrical BER floor translates directly into the BER floor of the optically modulated signal at 100 Gbaud.

For optical signal-to-noise ratio (OSNR) measurement, the modulator output optical signal is attenuated to different levels before being amplified, which produces the desired OSNR values, before entering the coherent receiver. The measured OSNR curves are plotted in Extended Data Fig. 4.

Microwave transmission line and velocity matching. Extended Data Fig. 5a, b shows the cross-sectional schematics of the integrated LN modulator and a conventional LN modulator. Extended Data Fig. 5c, d shows the numerically simulated microwave and optical field distributions. The simulations are performed using the finite element method (COMSOL Multiphysics). Owing to the high optical confinement (Extended Data Fig. 5d) in the thin-film LN platform, we can design the metal electrodes to be placed close to the waveguides (spacing <2.5 μm between metal and waveguide edge) without substantially increasing the optical losses (simulated metal absorption loss <0.03 dB cm⁻¹). We design the waveguide width, ridge height and metal gap to achieve a much higher electro-optic efficiency than conventional LN modulators.

More importantly, the SiO₂/Si-stack substrate in our platform can be independently designed as a microwave dielectric to realize optimal microwave-optical group velocity matching without sacrificing electro-optic overlap. In conventional LN modulators, velocity matching is a non-trivial task because of the large discrepancy between the dielectric constants of LN at microwave ($\epsilon_{RF} = 28$) and optical ($\epsilon_{opt} = 5$) frequencies. As a result, a buffer SiO₂ layer is used to overcome the large group-velocity mismatch between microwave and optical signals (Extended Data Fig. 5b), which further reduces the already suboptimal electro-optic efficiency. In our platform, we design the thickness of the buried SiO₂ layer and the material of the handle substrate (Si in this case) to achieve velocity matching without sacrificing electro-optic overlap. We design the coplanar waveguide signal linewidth and the substrate SiO₂ thickness such that the group refractive indices for microwave and optics are both approximately 2.2 (Extended Data Fig. 5e), and that the transmission line has an impedance near 50 Ω. The final device has a LN slab thickness of 300 nm, a buried SiO₂ layer thickness of 4.7 μm and a Si substrate thickness of 500 μm.

Modulator energy consumption. Because our modulator uses a transmission line configuration with a 50-Ω load, the electrical energy per bit dissipated in the modulator can be estimated as $W_e = V_{rms}^2 / (BR)$, where V_{rms} is the root-mean-square drive voltage, B is the bit-rate and R is the driver impedance¹⁶.

For direct CMOS modulation at 70 Gbit s⁻¹ (Fig. 2c, d), the electrical root-mean-square voltage $V_{rms} = 36$ mV, resulting in a low electrical energy consumption of 0.37 fJ bit⁻¹. For the 210 Gbit s⁻¹ data modulation in Fig. 3d, the electrical V_{rms} is 360 mV, resulting in an electrical energy consumption of 14 fJ bit⁻¹.

The energy consumption of the entire data-transmission system also includes the power consumption of CMOS DAC, laser, optical amplifiers and analogue-to-digital converter.

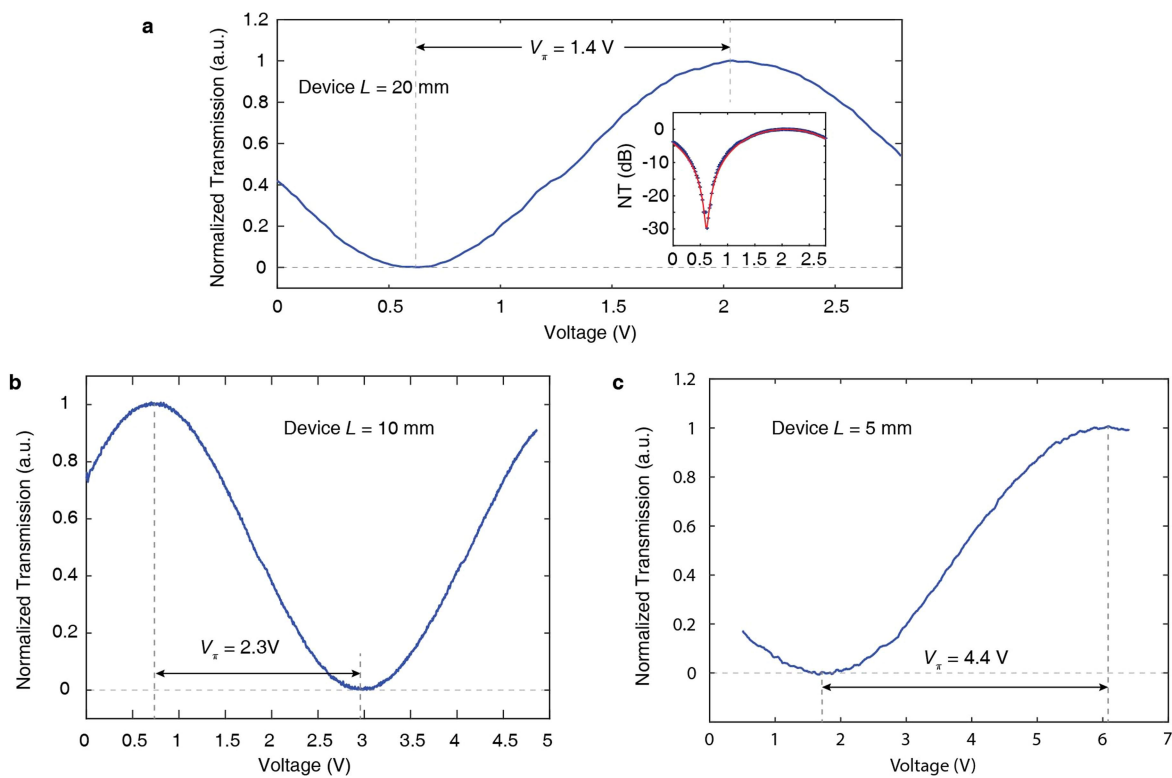
Modulator figures of merit comparison. Extended Data Table 1 lists the detailed numbers (V_π values, 3-dB electro-optic bandwidths and phase-shifter losses) and references of previously demonstrated thin-film LN modulators^{25,26,29,34,35}, commercial LN modulators^{36–38}, and modulators based on silicon^{39–42}, InP^{14,43,44}, polymers^{45,46} and plasmonics^{18,47,48}. These numbers are used in Fig. 4c, d. The loss numbers plotted in Fig. 4d consider only the loss of the active modulation regions, excluding the coupling and splitter losses, to provide a comparison of modulation-induced optical absorption between different material platforms and modulation schemes. In practical applications, other important performance merits, including footprint, extinction ratio, modulator linearity, thermal stability and power handling, should also be considered. Also, the comparison here is only on the device level. In practical data-transmission settings, the performance of other components, such as the driving circuits, also needs to be considered.

Data availability

The data sets generated and/or analysed during the current study are available from the corresponding authors on reasonable request.

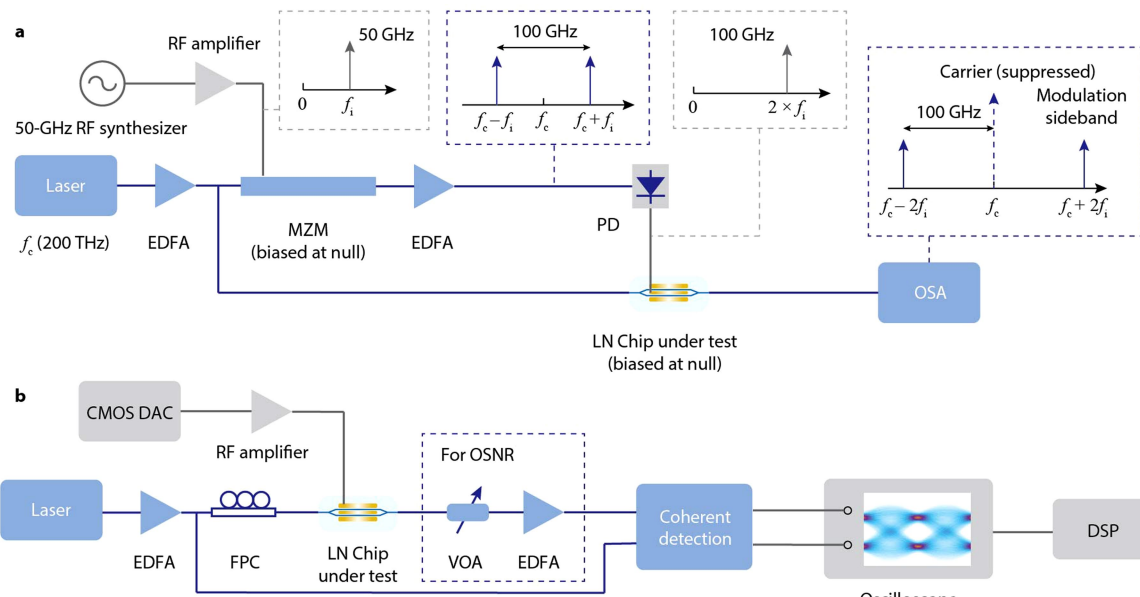
33. Winzer, P. J. & Essiambre, R. J. Advanced optical modulation formats. *Proc. IEEE* **94**, 952–985 (2006).
34. Mercante, A. J. et al. 110 GHz CMOS compatible thin film LiNbO₃ modulator on silicon. *Opt. Express* **24**, 15590–15595 (2016).

35. Jin, S., Xu, L., Zhang, H. & Li, Y. LiNbO₃ thin-film modulators using silicon nitride surface ridge waveguides. *IEEE Photonics Technol. Lett.* **28**, 736–739 (2016).
36. 100G/400G LN Modulator. <http://www.fujitsu.com/jp/group/foc/en/products/optical-devices/100gln/>
37. Eospace 2017 Advanced Products. <http://eospace.com/pdf/EOSPACEbriefProductInfo2017.pdf>
38. 40 GHz or 40 Gb/s Lithium Niobate Modulators. https://www.thorlabs.com/newgrouppage9.cfm?objectgroup_id=3948
39. Dong, P. et al. Monolithic silicon photonic integrated circuits for compact 100⁺ Gb/s coherent optical receivers and transmitters. *IEEE J. Sel. Top. Quantum Electron.* **20**, 150–157 (2014).
40. Thomson, D. J. et al. 50-Gb/s silicon optical modulator. *IEEE Photonics Technol. Lett.* **24**, 234–236 (2012).
41. Streshinsky, M. et al. Low power 50 Gb/s silicon traveling wave Mach-Zehnder modulator near 1300 nm. *Opt. Express* **21**, 30350–30357 (2013).
42. Azadeh, S. S. et al. Low V silicon photonics modulators with highly linear epitaxially grown phase shifters. *Opt. Express* **23**, 23526–23550 (2015).
43. Rouvalis, E. Indium phosphide based IQ-modulators for coherent pluggable optical transceivers. In *2015 IEEE Compound Semiconductor Integrated Circuit Symposium* 1–4 (2015); <https://doi.org/10.1109/CSICS.2015.7314513>
44. Letal, G. et al. Low loss InP C-band IQ modulator with 40 GHz bandwidth and 1.5 VV_π. In *2015 Optical Fiber Communications Conference and Exhibition* 1–3 (2015); <https://doi.org/10.1364/OFC.2015.Th4E.3>
45. Wolf, S. et al. Coherent modulation up to 100 Gb/s 16QAM using silicon-organic hybrid (SOH) devices. *Opt. Express* **26**, 220–232 (2018).
46. Alloatti, L. et al. 100 GHz silicon-organic hybrid modulator. *Light Sci. Appl.* **3**, e173 (2014).
47. Ayata, M. et al. High-speed plasmonic modulator in a single metal layer. *Science* **358**, 630–632 (2017).
48. Haffner, C. et al. All-plasmonic Mach-Zehnder modulator enabling optical high-speed communication at the microscale. *Nat. Photon.* **9**, 525–528 (2015).



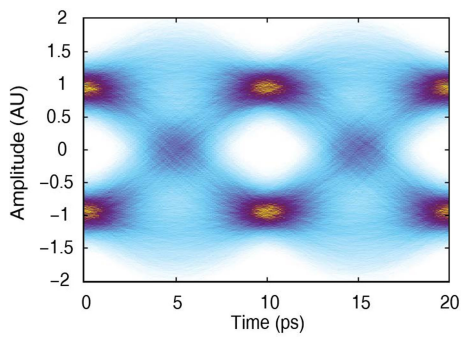
Extended Data Fig. 1 | Half-wave voltages of devices with different active lengths. a–c, Normalized optical transmission of the 20-mm (a), 10-mm (b) and 5-mm (c) device as a function of the applied voltage,

showing half-wave voltages of 1.4 V, 2.3 V and 4.4 V, respectively. The inset of a shows the measured normalized transmission (NT) on a logarithmic scale, revealing an extinction ratio of 30 dB.

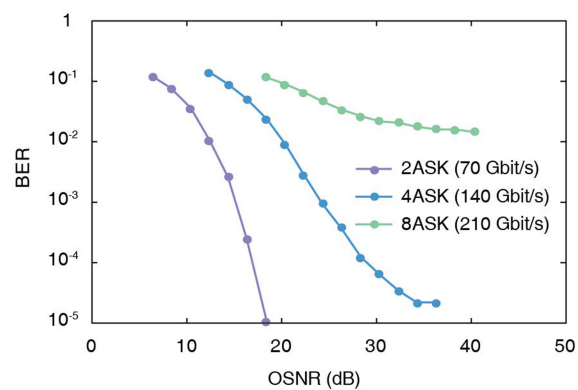


Extended Data Fig. 2 | High-speed measurement set-ups. **a**, Set-up for measuring the modulator electro-optic responses from 35 GHz to 100 GHz. **b**, High-speed data modulation set-up. For direct CMOS driving, the RF amplifier is bypassed. EDFA, erbium-doped fibre

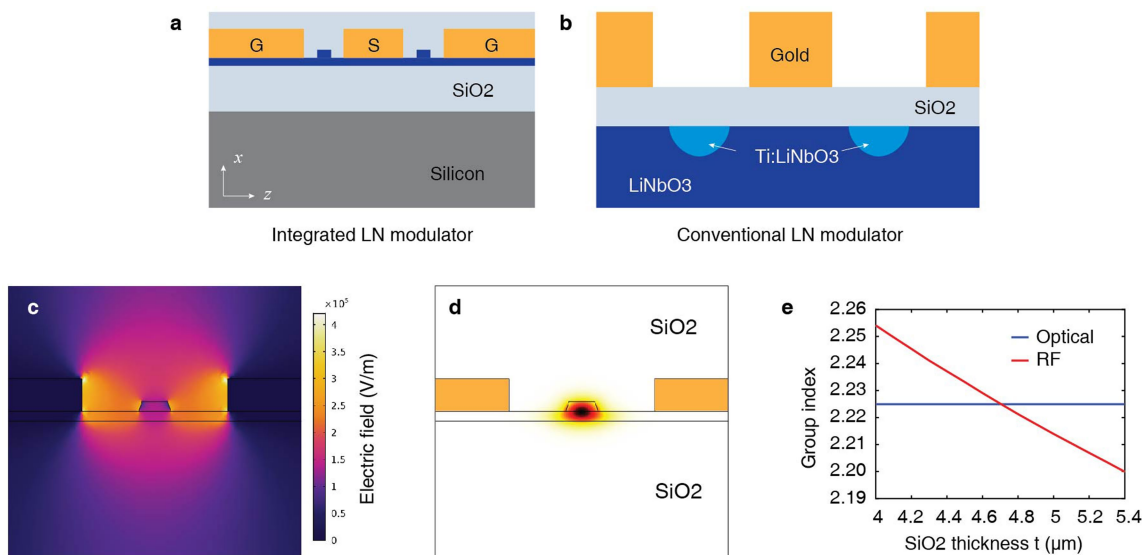
amplifier; FPC, fibre-polarization controller; MZM, Mach-Zehnder modulator (commercial); OSA, optical spectrum analyser; VOA, variable optical attenuator.



Extended Data Fig. 3 | Electrical eye diagram at 100 Gbaud. The measured electrical BER is 3.6×10^{-5} , limited by the signal distortion from the electronic circuit.



Extended Data Fig. 4 | OSNR measurements. BER versus OSNR for the three modulation schemes at 70 Gbaud.



Extended Data Fig. 5 | Comparison of integrated and conventional LN modulators. **a, b,** Schematics of the cross-sections of thin-film (**a**) and conventional (**b**) LN modulators. Our thin-film modulator (**a**) has an oxide layer underneath the device layer, so that velocity matching can be achieved while maximum electro-optic efficiency is maintained. A conventional modulator (**b**) also uses a buffer oxide layer for velocity matching, but on top of LN which further compromises the electro-optic

overlap. **c, d,** Numerically simulated microwave (**c**) and optical (**d**) field distributions (both shown in E_z components) in the cross-section of the thin-film modulator. For microwave simulations, the electric-field values are obtained when a voltage of 1 V is applied across the two electrodes. **e,** Group refractive indices for both optical and microwave signals as a function of the buried oxide thickness. Velocity matching can be achieved with an oxide thickness of about 4,700 nm.

Extended Data Table 1 | Comparison of modulator voltage, bandwidth and loss performance

Type	Half-wave voltage	Voltage-length product	3-dB electro-optic bandwidth	Phase-shifter loss	Reference
Thin-film LN	1.4 V	2.8 V·cm	45 GHz	0.4 dB	This work
Thin-film LN	2.3 V	2.3 V·cm	80 GHz	0.2 dB	This work
Thin-film LN	4.4 V	2.2 V·cm	100 GHz	0.1 dB	This work
Thin-film LN	4 V	3.1 V·cm	33 GHz	N/A	[26]
Thin-film LN	9.4 V	9.4 V·cm	40 GHz	1 dB	[34]
Thin-film LN	9 V	1.8 V·cm	15 GHz	0.6 dB	[25]
Thin-film LN	2.5 V	3 V·cm	8 GHz	8.4 dB	[35]
Thin-film LN	13 V	6.7 V·cm	100 GHz	7.8 dB	[29]
Commercial LN	3.5 V	>10 V·cm	35 GHz	N/A	Fujitsu, [36]
Commercial LN	4.5 - 4.9 V	>10 V·cm	30 - 40 GHz	4 dB	EO Space, [37]
Commercial LN	2.9 - 3.3 V	>10 V·cm	20 - 25 GHz	4 dB	EO Space, [37]
Commercial LN	5.5 V	>10 V·cm	35 GHz	N/A	Thorlabs, [38]
Silicon	10 V	2.4 V·cm	N/A	4.2 dB	[39]
Silicon	16 V	2.8 V·cm	N/A	3.2 dB	[40]
Silicon	8.5 V	2.6 V·cm	30 GHz	3.3 dB	[41]
Silicon	4.1 V	0.74 V·cm	34 GHz	7.6 dB	[42]
Indium Phosphide	2 V	N/A	40 GHz	6.5 dB	[43]
Indium Phosphide	1.5 V	0.6 V·cm	40 GHz	7.5 dB	[44]
Indium Phosphide	1.5 V	0.54 V·cm	67 GHz	2 dB	[14]
Polymer	2.2 V	0.11 V·cm	100 GHz	9.5 dB	[45]
Polymer	22 V	0.11 V·cm	100 GHz	2.5 dB	[46]
Plasmonics	20 V	N/A	110 GHz	2.5 dB	[18]
Plasmonics	12 V	0.012 V·cm	70 GHz	6 dB	[47]
Plasmonics	10 V	0.006 V·cm	70 GHz	2.5 dB	[48]

Detailed half-wave voltages, 3-dB electro-optic bandwidths and phase-shifter losses of commercial LN modulators, previously demonstrated thin-film LN modulators as well as modulators based on Si, InP, polymers and plasmonics with high bandwidths, are listed.